Research Paper

Changing the freezing interface characteristics to reduce the ice adhesion strength

Tingkun Chen [a], Xinju Dong [a], Liman Han [a], Qian Cong [a], Yingchun Qi [a], Jingfu Jin [a,*], Chaozong Liu [b], Mingqing Wang [c]

[a] College of Biological and Agricultural Engineering, Key Laboratory of Bionic Engineering (Ministry of Education), Jilin University, Changchun 130022, PR China
[b] Department of Ortho and MSK Science, University College London, London HA7 4LP, United Kingdom
[c] Institute for Materials Discovery, University College London, London WC1E 7JE, United Kingdom

ARTICLEINFO

Keywords:
Freezing process
Discontinuous characteristic
Interface
Freezing parameters
Ice adhesion strength

ABSTRACT

To mitigate the hazards of ice adhesion and reduce anti/de-icing costs, this study proposed a simple and low-cost anti/de-icing method. Different positions of the attached water's internal interface have different phase transformation times owing to changes in the thermal conductivity characteristics of the material surface. Consequently, the characteristic parameters of water during freezing can be used to reduce the ice adhesion strength. The mold method was used to coat low thermal conductivity silicone rubber with a striped and dotted circular pattern on the surface to change the thermal conductivity continuity of the material surface, and the ice adhesion strength on different samples being measured. Different characteristic parameters during the freezing process were measured using the tracing point method, the tangential freezing interface stress being measured using a purpose-built device. The results showed that a sample surface with a discontinuous distribution of silicone rubber could greatly reduce the ice adhesion strength. For example, compared with the ice adhesion strength on the normal surface of polymethyl methacrylate (PMMA) and an aluminum alloy, 142.95 and 150.22 kPA respectively, the use of PMMA and an aluminum alloy with a stripe coating reduced the ice adhesion strength by a maximum of 82.18% and 72.67%, respectively. When the attached water phased into ice, it was accompanied by the release of heat and an increase in volume. Meanwhile, the tangential interface stress increased instantaneously outward along the interface direction and tended to stabilize. A phase transition time difference was formed within the attached water by changing the thermal conductivity continuity of the material surface. The tangential freezing interface stress, heat released, and the increased volume formed by the adhering water located in the late-frozen region during the freezing process acted on the initially frozen region to destabilize the adhesion interface between it and the material surface; thus reducing the ice adhesion strength. Based on the results, it was evident that changing the thermal conductivity continuity of the material surface could actively reduce the adhesion strength. This study should be helpful in developing simple, low-cost, nonpolluting, and active anti/de-icing methods in the engineering field.

1. Introduction

In a low-temperature environment, water or moisture adheres the material surfaces and freezes. Under the anchoring effect, chemical bonds, and other factors [1–5], a stable adhesion interface between the ice and the material is formed, there being an inherent adhesion strength between the accumulated ice and the material which can make it difficult to remove the accumulated ice Although ice adhesion is a common natural phenomenon, it can change the morphology, transmittance, operational stability, and safety of the adhesion components. For example, the load of a transmission line increases when it is covered with ice, which can lead to the line fractures and potential tower collapse [6–8]. Ice accumulation on wing surfaces can change the aerodynamic lift-drag coefficient, affecting the maneuvering stability of the aircraft [9–10]. Moreover, ice accumulation on photovoltaic panel surfaces can reduce the photoelectric conversion efficiency [11–12].

Abbreviation: PMMA, polymethyl methacrylate.

* Corresponding author at: Jilin University, No.5988 Renmin Street, Changchun 130022, PR China.
E-mail address: jinjingfu@jlu.edu.cn (J. Jin).

Consequently, ice adhesion can have serious implications in people's lives, causing notable socioeconomic losses.

Water can be a special adhesive in a low-temperature environments, and the ice formed by water freezing and the material itself forming an adhesion system. In short, water or moisture, a low-temperature environment or interface, and a substrate are required for ice to adhere to a material surface. Based on these conditions, researchers have developed several anti/de-icing technologies to mitigate the hazards of ice accumulation [13]. The principles of existing anti/de-icing methods can be summarized into several categories—that is, changing the composition of water to reduce its freezing point, increasing the surface temperature to delay the freezing time of water, modifying the material wettability to reduce the adhesion effect of water or the ice adhesion strength, and removing accumulated ice via direct removal or heating [14–16]. However, existing anti/de-icing methods have certain disadvantages in their practical use. For example, chemical methods that change the freezing point of water can cause component corrosion, soil hardening, and water pollution [17–18]; and thermal methods to improve the surface temperature or melt the accumulated ice can consume considerable energy, increasing the cost of anti/de-icing [19–23]. In recent years, researchers have devoted themselves to fabricating superhydrophobic surfaces or coatings that affect the water adhesion or decrease the ice adhesion strength. Superhydrophobic surfaces are promising anti/de-icing method owing to their significant water-repellency or ability to decrease the ice adhesion strength [24–25]. However, superhydrophobic surfaces do not always maintain their superhydrophobicity characteristics [26–33]. Farhadi *et al.* [28] and Kulinich *et al.* [30] repeatedly measured the ice adhesion strength on 6061 aluminum and found that the ice adhesion strength gradually increased with increasing test time. The composition of the superhydrophobic surface could also change with increasing icing and de-icing cycles [28,30,34]. Moreover, other studies have reported that superhydrophobic surfaces can exhibit defects, including poor mechanical properties and easily damaged surface structures [24,34–36]. The preparation of super-hydrophobic surfaces can also be complicated and expensive [37]. Hence, it is urgently developed a kind of anti/de-icing method with no pollution, inexpensive, low energy consumption, and simple preparation in the engineering field.

After thousands of years of evolution, organisms have formed optimal structures to adapt to their living environments. For example, the desert beetle uses the discontinuous wettability and morphology of its body surface to collect water [38], while dung beetles, earthworms, mole crickets, and other organisms have discontinuous surface morphology can move in wet soil without clay [39–43]. Consequently, the discontinuous characteristics of the organism surface can provide a reference for developing anti/de-icing technologies.

As a special adhesive and phase change energy storage material, water can attach to material surfaces under cold conditions, accompanied by a phase change, the release of heat, and an increase in volume, the accumulated ice forming an adhesive system with the substrate. The surface characteristics of the substrate can affect the ice adhesion strength, such as surface roughness, wettability, etc [1,44–45]. Moreover, water or ice and materials have different linear expansion coefficients, and the phase change that occurs during the freezing process creates tangential stress at the ice interface [46].

By learning the discontinuity of biological surface characteristics, the surface thermal conductivity continuity was changed to affect the freezing sequence of water adhering to a material surface. It meant that the time required to form tangential interfacial stresses during the freezing process varied for different regions of attached water. The adhesive stability between the accumulated ice and the substrate could be influenced, affecting the ice adhesion strength on the material surface. The freezing process on different surface characteristics was observed using a custom-made device, and the ice adhesion strength on normal and discontinuous surfaces was measured. Combined with the freezing process of water on the material surface, the influence of the discontinuous thermal conductivity surface on the ice adhesion strength was analyzed. Consequently, the results of this study could provide a reference for the development of anti/de-icing methods.

2. Materials and methods

2.1. Materials

Silicone rubber has been widely used in the medical, automotive, and other engineering fields owing to its good weather resistance, low cost, chemical stability, strong adhesion, and other characteristics [47]. In this study, RTV-1 silicone rubber (purchased from Guangdong Hengda New Material Technology Co., Ltd.) was coated at different positions on the substrate surface to change the continuity and unity of the material's thermal conductivity. PMMA and 6061 aluminum—which are widely used in the engineering field—were used as the substrates during the experiment. The thermal conductivities of 6061 aluminum alloy (Haerbin Dongbeilong Metal Co., Ltd.), PMMA (Ju Yayuan Plastic Materials Co., Ltd.), and silicone rubber were 167, 0.2, and 0.13 W/m k, respectively [47–48].

2.2. Sample fabrication

Non-continuously coated silicone rubber on the sample surface was fabricated using the mold method, as shown in Fig. 1. A flexible film is pasted onto the substrate surface, and the pattern on which the silicone rubber needs to be coated being processed using a laser. The silicone rubber is coated and cured naturally at room temperature for 24 h. The film is then removed, the substrate surface being wiped down with alcohol. A flexible film is used to control the thickness of the silicone rubber coating, and the thickness of the flexible film is 0.02 mm.

The adhesion grade of the silicone rubber on the material surface is measured using a bagel knife according to the standard [49]. The adhesion grade of the silicone rubber on the surfaces of PMMA and aluminum alloy is 5B.

2.3. Experimental device and methods

2.3.1. Adhesion strength tests

In the engineering field, the tangential adhesion strength between ice and a material can affect the removal of accumulated ice. Consequently, the ice adhesion strength was measured and the influence of the discontinuous surface characteristics on the ice adhesion strength was analyzed.

The method was used to discontinuously coat the surfaces of PMMA and aluminum alloy with silicone rubber distributed as discrete dots and stripes. The diameter of the silicone rubber distributed as discrete dots was 3 mm, the circle center distance was 4 mm, and the distribution patterns were 4, 9, and 16 dots. The strip size of the silicone rubber coated on the material surface was 20 × 3 mm (L × W), the spacing was 1 mm. The numbers of strip distributions were two, three, and four. The thickness of the silicone rubber coating on the sample surface was 0.02 mm. The shape of the silicone rubber coatings on the sample surface was as shown in Fig. 2.

The sample descriptions are listed in Table 1, all samples have dimensions of 50 × 50 × 8 mm (L × W × H). As shown in Table 1, a normal surface is meant that the surface is not coated with silicone rubber.

During the test, an aluminum alloy cup was placed at the center of the sample using a placement tool, as shown in Fig. 3**(a)**, after which five milliliters of water were injected into the aluminum cup. The entire test model was placed in a climate chamber that controlled the experimental temperature, maintaining it at −20 ℃. The temperature control accuracy of the climate chamber is ±0.01 °C. After freezing for 1 h, the tangential ice adhesion strength on the different sample surfaces was measured using the method shown in Fig. 3**(b)**. The maximum pulling force of accumulated ice during the stripping process was measured. The

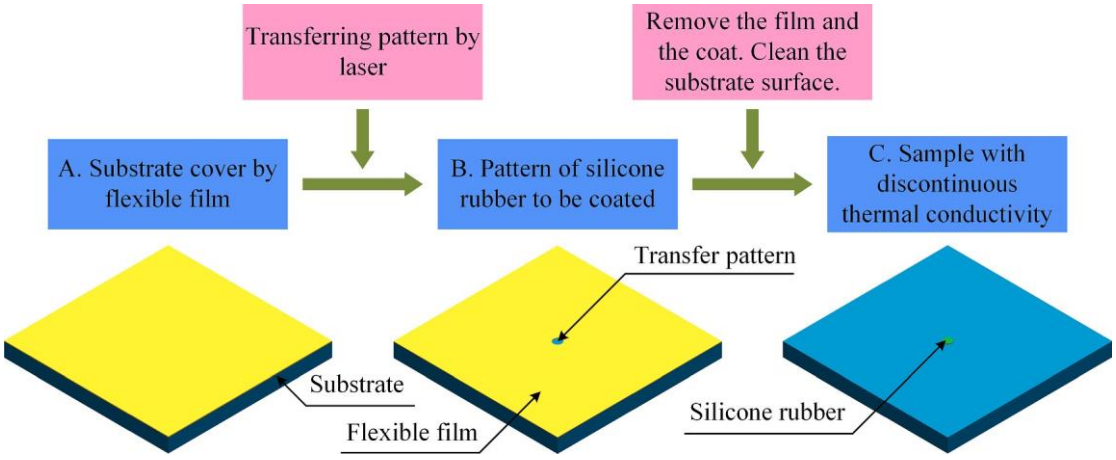

Fig. 1. Preparation of samples with discontinuous thermal conductivity using the mold method.

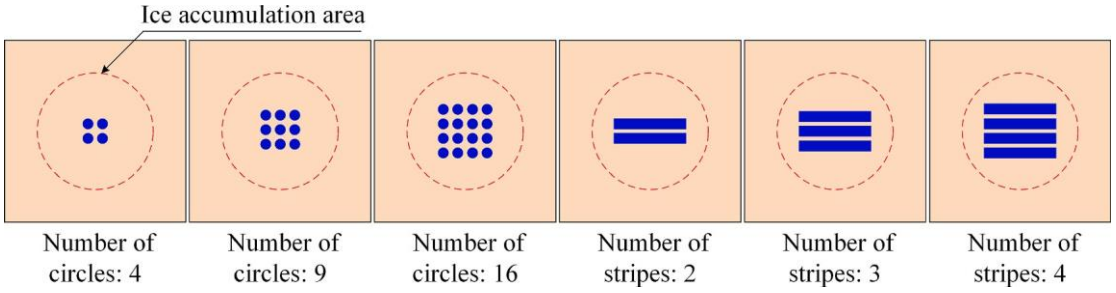

Fig. 2. Coating shapes of silicone rubber on the sample surface.

Table 1
Sample descriptions.

Substrate	Normal surface	The substrate surface with silicone rubber					
		Number of stripes			Number of circles		
		2	3	4	4	9	16
PMMA	A_{PMMA}	A^2_{PMMA}	A^3_{PMMA}	A^4_{PMMA}	B^4_{PMMA}	B^9_{PMMA}	B^{16}_{PMMA}
Al	A_{Al}	A^2_{Al}	A^3_{Al}	A^4_{Al}	B^4_{Al}	B^9_{Al}	B^{16}_{Al}

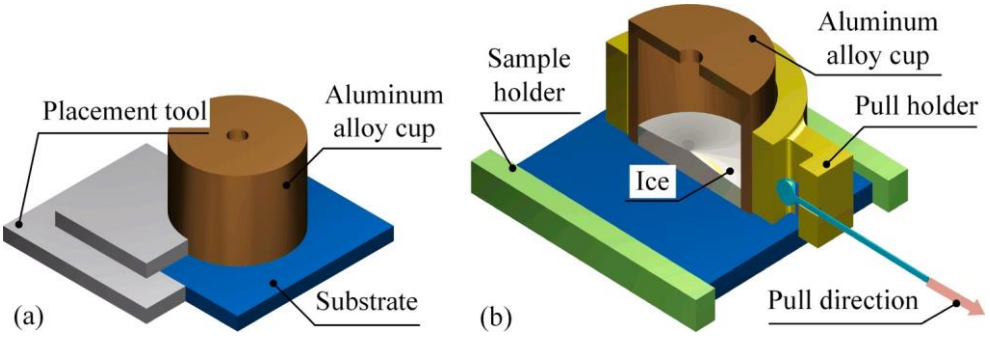

Fig. 3. Details of ice adhesion strength measurement test. (a) Aluminum alloy cup placement details; (b) Schematic diagram of tangential ice adhesion strength test.

tangential ice adhesion strength could be calculated using the equation $P = F/S$, where P denotes the shear ice adhesion strength, F denotes the maximum pulling force, and S denotes the inner area of the aluminum alloy cup. The inner diameter of the aluminum cup is 32 mm, and the accuracy of the draft gauge is 0.01 N.

2.3.2. Droplet freezing process

The influence of the silicone rubber on the freezing of water droplets on the sample surface was studied using the device shown in Fig. 4. The sample is cooled using a semiconductor based on the Peltier effect, and the power of the semiconductor is changed by adjusting the applied voltage. During the freezing process, a K-type temperature sensor is placed inside the droplet without touching the substrate surface to

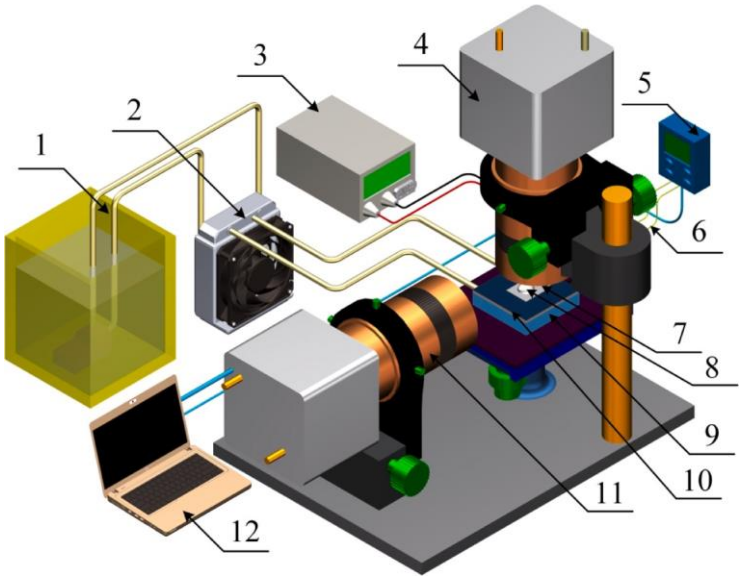

1. Water-cooled pool; 2. Cooling fan; 3. DC power supply; 4. CCD camera; 5. Temperature collector; 6. K-type temperature sensor; 7. Sample; 8. Water droplet; 9. Refrigeration stage; 10. Semiconductor; 11. Microscope; 12. PC.

Fig. 4. Observation device for the freezing process.

measure the transient response of the internal temperature of the droplet. The change in the water/ice appearance is recorded in real time using a CCD camera. The K-type temperature sensor has a diameter of 0.15 mm, its accuracy is ±0.1 °C.

The sample surface was cleaned in an acetone ultrasonic bath for three minutes and then in a deionized water ultrasonic bath for another three minutes. The samples were then oven dried at 30 ℃. During the observation test, the initial temperature of the sample surface was that of the ambient temperature (approximately 20 ℃), and the sample surface temperature was first set at −10 ℃. Five microliters of deionized water were then dropped onto the sample with a thickness of 0.5 mm using a micro pipettor. The freezing process of the PMMA and aluminum alloy, with and without silicone rubber, were observed using the self-made observation device. The coating thickness of the silicone rubber on the substrate was 0.02 mm.

2.3.3. *Interface stress during the freezing process*

A purposely-built test device was used to collect the tangential stress formed at the freezing interface during the freezing process, as shown in Fig. 5. Here, the tangential interface strain of water formed during the freezing process is measured indirectly, a circular strain gauge is attached to the center of the one side of the thin aluminum alloy plate, placed entirely within the environmental chamber. After wiping the surface of the aluminum alloy plate with ethanol, 1 ml of deionized water is dripped onto its surface. The freezing interface strain is then measured using a dynamic strain collector and transmitted to the collection terminal.

During the tests, the acquisition frequency of the system was set at 20 Hz. The strain of the aluminum alloy without water adhering to the surface in a low-temperature environment was collected simultaneously. The thin aluminum alloy plate was 50× 50× 0.5 mm (L× W× H). A circular strain gauge (Model: BHF350-12KA) was purchased from Taizhou Huangyan Electronic Components Co., Ltd.

3. Results

3.1. *Ice adhesion strength*

Fig. 6 shows the ice adhesion strength of the specimen surface after repeated tests, and the reduction rate of the ice adhesion strength on the anti/de-icing specimen surface relative to the ice adhesion strength on the normal specimen surface is calculated. Except for sample B^4, the ice

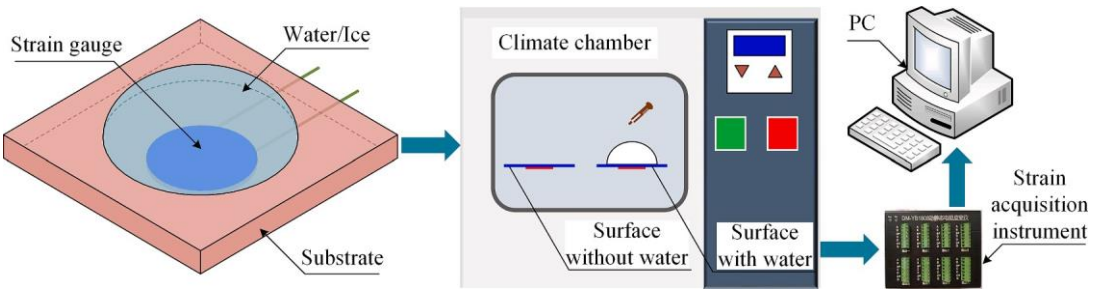

Fig. 5. Interface strain acquisition system.

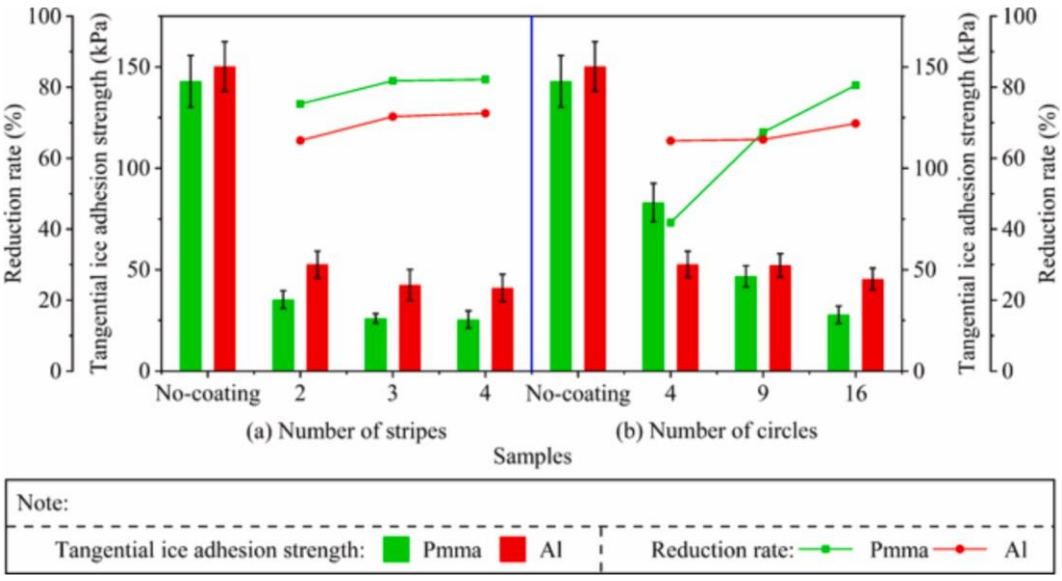

Fig. 6. Ice adhesion strength on different samples.

adhesion strength on the PMMA surface is lower than that on the aluminum alloy surface, regardless of the normal samples or anti/de-icing specimens with discontinuously coated silicone rubber. Moreover, the specimens coated with striped and dotted circular silicone rubber reduced the tangential ice adhesion strength, and the ice adhesion strength on the sample surface coated with the striped silicone rubber is lower than that of the sample surface coated with the dotted circular silicone rubber. It is evident that the coating shape of the silicone rubber on the aluminum alloy surface has little effect on the ice adhesion strength.

With increasing numbers of stripes or circles coated with silicone rubber on the sample surface, the ice adhesion strength on the sample surface decreases gradually. When the silicone rubber is coated in a striped pattern on the material surface, the ice adhesion strength on the A^4_{PMMA} surface is the lowest (25.47 kPa). The ice adhesion strength of the A^2_{Al} surface is the largest, and the reduction rate of the ice adhesion strength is 64.97%. When the sample surface is coated with 3 or 4 strips of silicone rubber, the difference between the ice adhesion strength of the two kinds of samples is small. For example, the reduction rate of ice adhesion strength on the surface of A^3_{Al} and A^4_{Al} is 71.71% and 72.67%, respectively.

When the material surface is coated with circular silicone rubber, the volume of circular silicone rubber has a greater influence on the ice adhesion strength of the PMMA than that of the aluminum alloy. Among the samples with round silicone rubber on the surface, the ice adhesion strength of the B^{16}_{PMMA} surface is the lowest (27.80 kPa); the ice adhesion strength of the B^4_{PMMA} surface is the largest, and the reduction rate of the ice adhesion strength is 41.84%. When dotted circularly coated silicone rubber on the aluminum alloy surface numbers four or nine, the difference between the two sample surfaces is small. For example, the ice adhesion strength on B^4_{Al} and B^9_{Al} is 64.91 kPa and 65.28 kPa, respectively.

3.2. Freezing process on the sample surface with discontinuous properties

The freezing processes on different sample surfaces were observed using the device shown in Fig. 4. As shown in Fig. 7, the freezing process of water on the surfaces of the different specimens is similar, regardless of whether the substrate is PMMA or an aluminum alloy. During the test, the freezing process of the water on the material surface can be summarized as follows—that is, the initial state, spreading state, and phase change until completely frozen. However, when the substrate surface is coated with silicone rubber, the contact diameter between the water and silicone rubber does not change much during the freezing process. This is evident in the freezing process observation test in the horizontal direction, as shown in Fig. 4. When the attached water is completely frozen on the ice, the height of the ice is greater than that of the initial water droplets.

3.2.1. Morphological characteristic parameters

To analyze the influence of the discontinuous silicone rubber coating on the ice adhesion strength, different morphological characteristic parameters of the freezing process were calculated. It is evident from the vertical direction shown in Fig. 7 that the contact area between the water and material is approximately circular. The freezing observation test shows that water undergoes the same freezing process on different material surfaces. Consequently, the tracing point method can be used in experiments to calculate the morphological characteristic parameters of water during the freezing process on a normal aluminum alloy surface. This method has been validated by several studies [34,50–54].

Fig. 8 shows the morphological characteristics of the water droplet attached to the aluminum alloy surface to be measured during the freezing process, where Fig. 8**(a) and 8(b)** show the initial state of the water on the material surface and the steady state after freezing.

Fig. 9 shows the variation in the morphological parameters of water during the freezing process on the normal aluminum alloy surface compared with the initial state. After water was titrated onto the material surface, it starts to spread. Compared with the initial state, the contact diameter between the water and material surface increases gradually. Because the volume of attached water does not change, its height gradually decreases before freezing, and the cross-sectional diameter at one-third of the droplet height gradually increases. Moreover, the cross-sectional diameter at two-thirds of the droplet height gradually decreases, as shown in Fig. 9.

When the attached water droplet enters a phase change, the cold surface restricts the increase in the contact diameter. As shown in Fig. 7, a freezing front appears within the attached water during the freezing process, the area behind the front freezing. When the freezing front moves to one-third of the droplet height, the cross-section is frozen, and the cross-sectional diameter being constrained. It is well known that the water volume increases after freezing. Moreover, the internal temperature of the droplet increases abruptly within seconds of the phase transition [13,51].

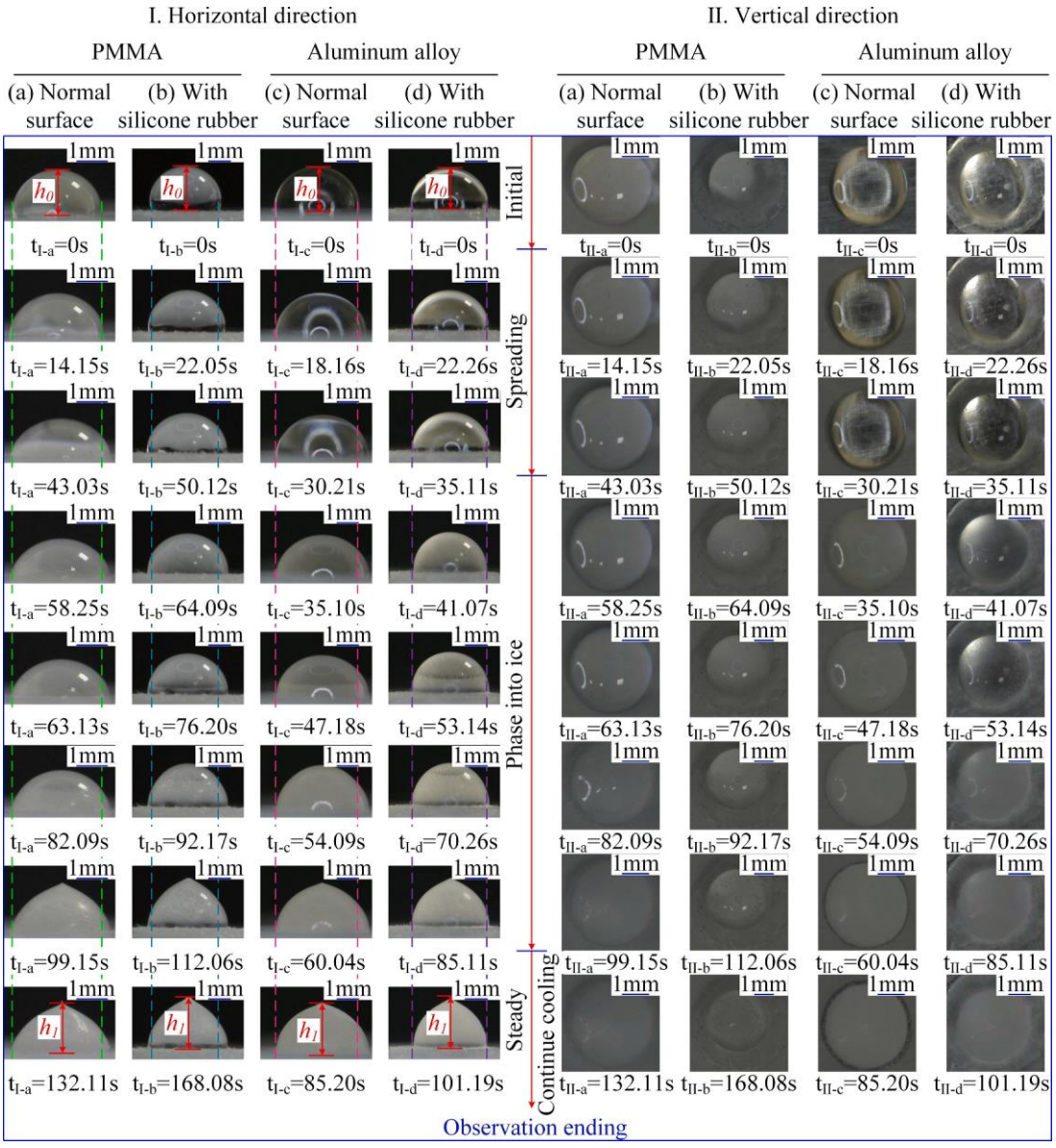

Fig. 7. Freezing process on different substrates.

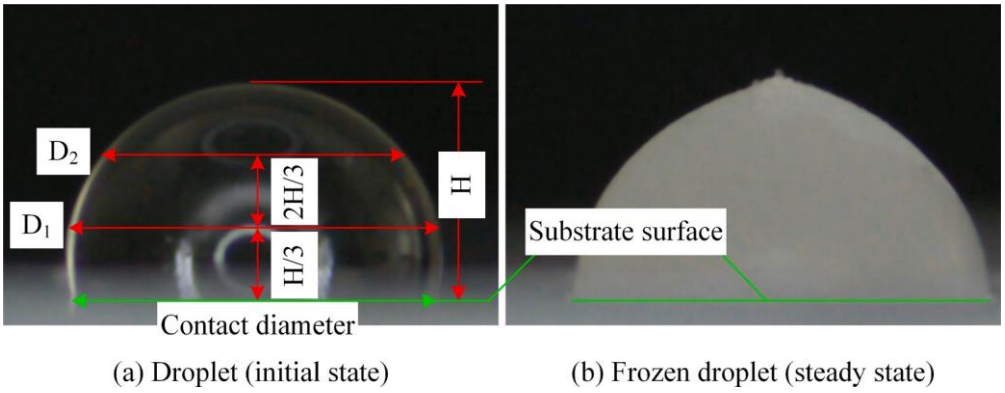

Fig. 8. Measurement location of water/ice morphological characteristics during the freezing process.

Consequently, with the continuous upward movement of the freezing front, the height and cross-sectional diameter at two-thirds of the droplet height increases instantaneously, increasing the volume. When the attached water is completely frozen, changes in the morphological characteristic parameters are not significant.

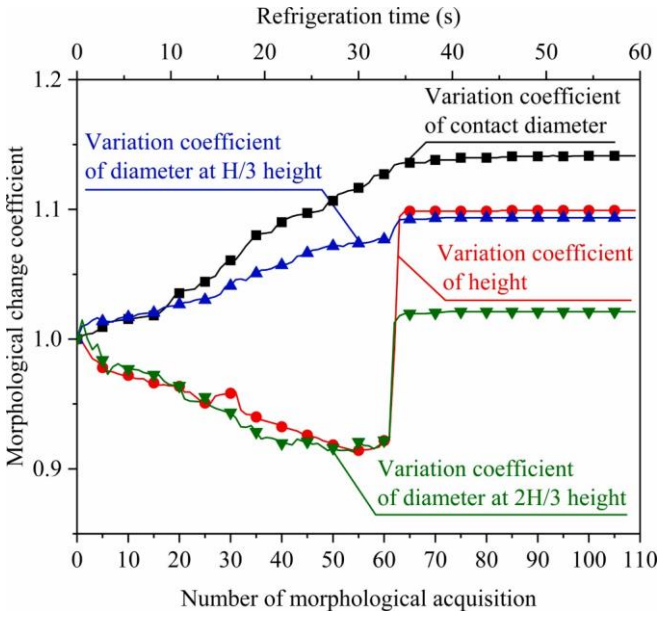

Fig. 9. Changes in morphological parameters of water during the freezing process on the normal Aluminum alloy surface.

3.2.2. Changes in the internal temperature during the freezing process

As the freezing process was observed using the device shown in Fig. 4, the internal temperature of the water during the freezing process on different specimen surfaces was measured, as shown in Fig. 10. Compared to the normal surface, the coated silicone rubber delays the phase transition time of the water on the surface. Because the thermal conductivity of the PMMA substrate is lower than that of the aluminum alloy, the phase transition time of water on the aluminum alloy surface with or without the silicone rubber coating is shorter than that of water on the PMMA surface with or without the silicone rubber coating.

To verify the effect of the discontinuous distribution of silicone rubber on the freezing process, the freezing of water on the specimen surface with discontinuously distributed silicone rubber was observed in the vertical direction. Silicone rubber was discontinuously coated onto the aluminum alloy surface using the method shown in Fig. 1. The coating diameter of the silicone rubber was 5 mm, the spacing between adjacent silicone rubbers was 8 mm, as shown in Fig. 11. During the test, 5 ml of deionized water was titrated onto the surface to completely cover the non-continuously coated silicone rubber, and the target temperature of the aluminum alloy surface being set to —10 °C. The size of the substrate was 40 × 40 × 0.5 mm (L × W × H).

Fig. 11 shows the freezing process of water on a specimen surface with a discontinuous silicone rubber coating. It is evident that the coated silicone rubber changes the freezing order within the attached water, which can be seen by the color of the different locations during the freezing process. Moreover, the freezing time of water attached to the silicone rubber-coated area is lesser than that in the normal area.

3.3. Tangential freezing interface stress

Based on the relationship between strain and stress, the strain at the freezing interface of water attached to the aluminum alloy surface during freezing can be determined. During the tests, the strain direction was defined as positive along the surface of material. The test ambient temperature was reduced from the ambient temperature (approximately 20 ℃) to -20 ℃ using the climate chamber. When the water was completely frozen, the environment temperature was reset to 20 ℃.

Fig. 12 shows the change in the freezing interface strain during the freezing-thawing process of 1 ml of deionized water on the aluminum alloy without coating with silicone rubber using the device shown in Fig. 5. The freezing interface strain generated by the two specimens gradually returns to the initial state at the end of the test; consequently, the measurement and collection of the freezing interface strain can be performed using the method shown in Fig. 5.

As shown in Fig. 12, the change process of the interfacial strain of the aluminum alloy with water on the surface can be divided into three stages: a decrease in strain, and a stabilization phase after an increase in strain with the decreasing of ambient temperature. When the ambient temperature reaches -20 °C, the interfacial strain formed by the aluminum alloy without water on the surface no longer decreases, tending to stabilize. When the ambient temperature increases, the interfacial strain formed by the sample with water on the surface fluctuates before gradually returning to its initial state.

Moreover, with a decrease in the ambient temperature (Fig. 12) the interface strain formed by the sample with water on the surface can be regarded as the tangential interface strain formed by water during the freezing process, relative to the change in the interface strain of the sample without water. Consequently, the difference between the interfacial strain formed by the specimen with water on the surface and that formed by the normal specimen is the tangential interfacial strain formed by the attached water during the freezing process. As shown in Fig. 12, the tangential freezing interface strain gradually increases as the ambient temperature decreases, tending to stabilize after fluctuation.

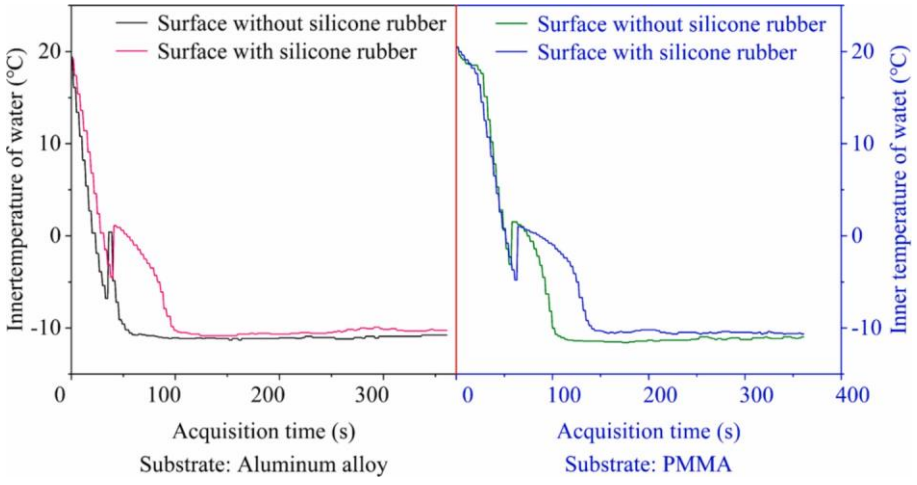

Fig. 10. The internal temperature during the freezing process.

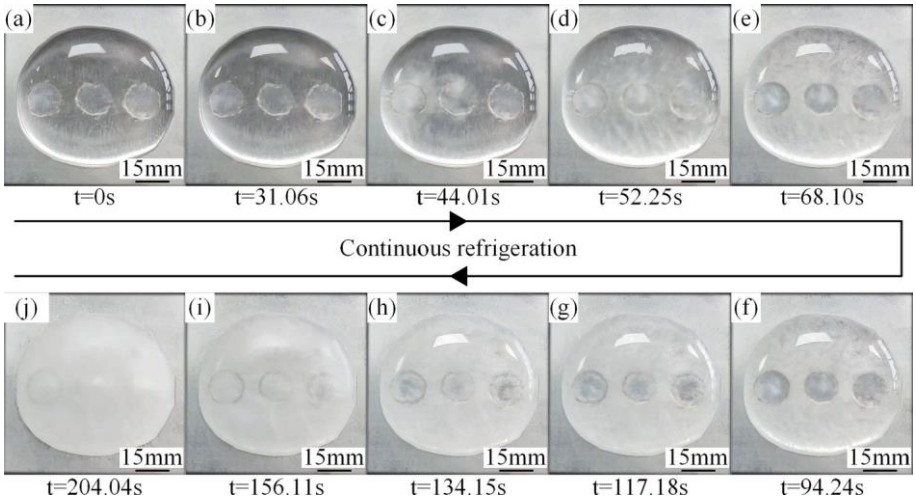

Fig. 11. Freezing process on aluminum alloy surface with discontinuous coated silicone rubber.

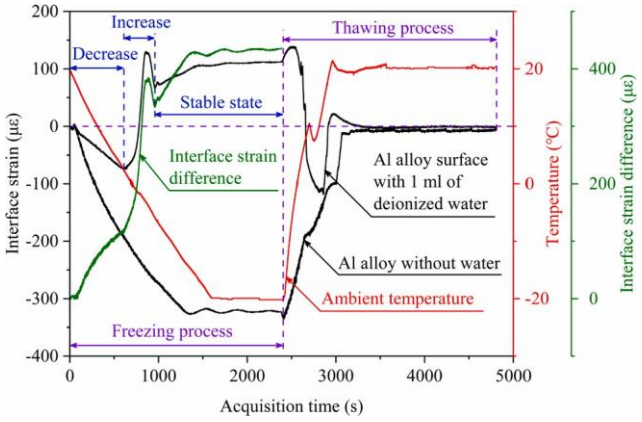

Fig. 12. Tangential interface strain during the freezing process.

4. Discussion

It is evident from the freezing process, morphological parameters, and internal temperature of water on the different sample surfaces that the freezing process of water on the material surface can be divided into the initial stage, supercooling, phase transformation, and completely frozen stages. The phase change is accompanied by an increase in volume and an abrupt change in the internal temperature, as is evident from Fig. 7, Fig. 9, and Fig. 10. The interface contact diameter and water droplet height are in the direction of the expansion change during the phase change process. As shown in Fig. 9, the contact diameter gradually decreases as the ambient temperature decreases, and the water and aluminum alloy being precooled and shrinking. Thus, the interfacial strain is reduced. The contact diameter increases rapidly during the phase change of the attached water, causing a rapid increase in the freezing interface strain. When the attached water is completely frozen, the contact diameter and interfacial strain do not change much. The effect of the discontinuous distribution of silicone rubber on the substrate surface on the ice adhesion strength can be explained by combining the freezing process, changes in morphology and internal temperature, and interfacial strain.

To explain the effect of discontinuous thermal conductivity characteristics on the test results, a theoretical model was proposed, as shown in Fig. 13. Water is attached to the material surface with a non-continuous distribution of silicone rubber (Fig. 13**(a)**), the water adherence interface being divided into silicone rubber surfaces and surfaces without silicone rubber. To facilitate the distinction, the area without silicone rubber is named **Area I**, and the silicone rubber surface is named **Area II**, as shown in Fig. 13**(b)**. Different locations within the attached water on the surface of the material have different freezing times—that is, the freezing sequence forms inside the attached water. As shown in Fig. 10, the freezing time of the water attached to the silicone rubber surface is shorter than that of water attached to the conventional surface. With a decrease in the ambient temperature, the water and substrate shrink, resulting in an inward shrinkage interface strain, as shown in Fig. 12. As the cooling continues, the attached water on the surface of **Area I** starts to phase change and expand, forming freezing interface stress along the interface direction outward, as shown in Fig. 13**(c)**. The released heat of the phase change also plays a role in delaying the freezing of the phase change of water attached to the surface of **Area II**.

When the phase transition of the adherent water on the surface of **Area I** is completed, the water attached to the surface of **Area II** is in a subcooled state, as is evident in Fig. 11. When the water phase change on the surface of the adjacent **Area I** freezes, the ice adhesion strength is formed between it and **Area II**, as shown in Fig. 13**(d)**. With continuous refrigeration, the ice adhesion strength formed by freezing the attached water near the surface of **Area I** on the material surface gradually increases, as shown in Fig. 13**(e)**. The ice covering the surface of **Area I** forms a constraint boundary to the attached water on the surface of **Area II**. However, when the adherent water on the surface of **Area II** enters the phase transformation stage, the tangential interface stresses outward along the interface direction acts on the surrounding frozen area and destroys the stability of the formed adhesive interface between the ice and **Area I**. Similarly, it is evident from Fig. 9 that the height direction also changes and increases during the freezing process. Consequently, the water attached to the surface of **Area II** exerts the normal phase expansion stress on the frozen area during the freezing process, further destroying the adhesion stability between the ice and **Area I**, reducing the ice adhesion strength, as shown in Fig. 13**(f)~(h)**. The heat released by the water on the surface of **Area II** during the freezing acts on the frozen area, affecting the adhesion strength between the ice and **Area I**.

The water attached close to the surface of **Area II** is completely frozen, as shown in Fig. 13**(i)~(j)**, the effect on ice adhesion stability and ice adhesion strength on the surface of **Area I** decreasing gradually. With continuous cooling, the adhesion strength between the ice and the substrate doses not change significantly.

There is a large difference in thermal conductivity between PMMA and the aluminum alloy, and a smaller difference in thermal conductivity between the PMMA and the silicone rubber. Consequently, the phase transformation time of water on the aluminum alloy surface with

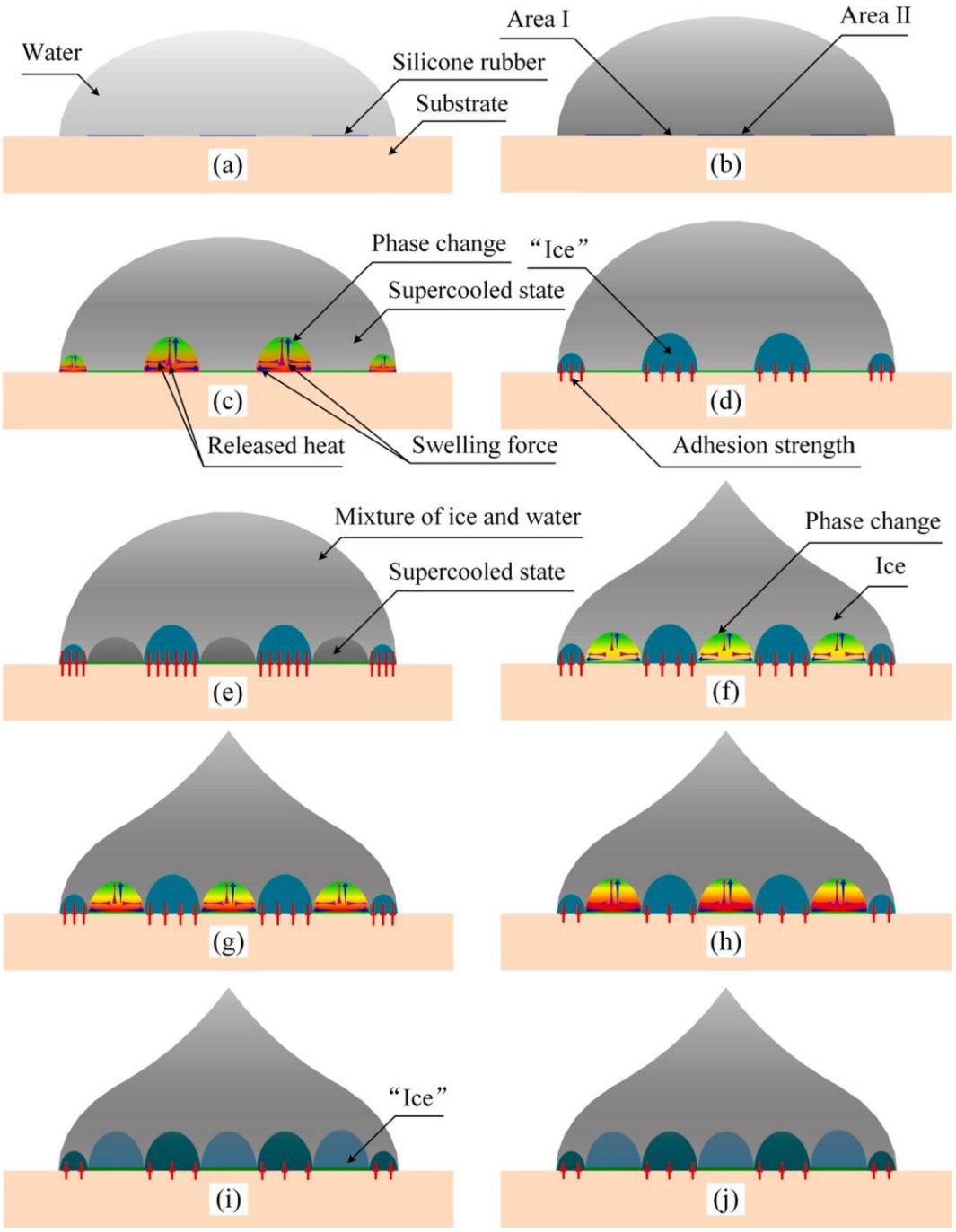

Fig. 13. Effect of surface discontinuous thermal conductivity on freezing process and ice adhesion strength.

and without the silicone rubber distribution is shorter than that of water on the sample surface with PMMA as the substrate, as is evident from Fig. 10. When the adhesion stability between the ice and material surface is destroyed by the phase change of the attached water on the **Area II** surface of the aluminum alloy, the adhesion interface between the ice and the aluminum alloy surface reforms with continued refrigeration. Consequently, the ice adhesion strength on the aluminum alloy surface with a discontinuous distribution of silicone rubber is greater than that on the PMMA surface with a discontinuous distribution of silicone rubber. Moreover, the shape of the silicone rubber coating on the aluminum alloy surface has little effect on the ice adhesion strength.

5. Conclusions

Silicone rubber with a low thermal conductivity was coated onto a material surface in the form of stripes and dots to alter the continuity of the thermal conductivity characteristics of the material surface. The ice adhesion strength test results showed that the sample with discontinuously distributed silicone rubber could greatly reduce the ice adhesion strength on the material surface relative to the normal sample without silicone rubber coating. The ice adhesion strength on the PMMA and aluminum alloy without silicone rubber coating was 142.95 and 150.22 kPA, respectively, while that on the PMMA and aluminum alloy surfaces with the striped coating could reached 25.47 and 41.05 kPa, respectively. The average ice adhesion strength on the PMMA and aluminum alloy surfaces with the dotted circular coating was 27.80 kPa and 45.41

kPa, respectively. Subsequently, a test device was designed to study the influence of discontinuous thermal conductivity characteristics on the ice adhesion strength. The freezing process of water on different sample surfaces was observed, the morphological characteristics parameters of water during the freezing process on the aluminum alloy surface were calculated, and the interfacial stress of water during the freezing process on the material surface was collected.

The continuity of the thermal conductivity characteristics of the material surface could be changed by the discontinuously distribution of the low thermal conductivity silicone rubber on the material surface. That was, the consistency of the freezing time of the water attached to the material surface during the freezing process could be changed so that different locations within the attached water would have different freezing sequences. The tangential interfacial stresses, expanded volume, and heat released during the freezing process in the late-frozen region were used to disturb the stability of the ice adhesion on the material surface, such that the ice adhesion strength on the material surface could be reduced.

Based on the experimental results, this study should be helpful in developing new low-cost active anti/de-icing methods for the engineering field with high anti/de-icing efficiency and minimal pollution. Moreover, change in surface wetting continuity, change in elastic continuity, and the coupling between different surface characteristics, could be used to improve the anti/de-icing efficiency.

Declaration of Competing Interest

The authors declare that they have no known competing financial interests or personal relationships that could have appeared to influence the work reported in this paper.

Data availability

No data was used for the research described in the article.

Acknowledgments

This work was supported by the National Natural Science Foundation of China (Grant No. 52205309); the Department of Science and Technology of Jilin Province, China (Grant No. 20220101215JC).

References

[1] F. Guerin, C. Laforte, M.I. Farinas, et al., Analytical model based on experimental data of centrifuge ice adhesion tests with different substrates, Cold Reg. Sci. Tech. 121 (2016) 93–99, https://doi.org/10.1016/j.coldregions.2015.10.011.
[2] V.F. Petrenko, S. Peng, Reduction of ice adhesion to metal by using self-assembling monolayers (SAMs), Can. J. Phys. 81 (1–2) (2003) 387–393, https://doi.org/10.1139/p03-014.
[3] I.A. Ryzhkin, V.F. Petrenko, Physical mechanisms responsible for ice adhesion, J. Phys. Chem. B. 101 (32) (1997) 6267–6270, https://doi.org/10.1021/jp9632145.
[4] H. Saito, K. Takai, G. Yamauchi, Water- and ice-repellent coatings, Surf. Coat. Int. 80 (4) (1997) 168–171, https://doi.org/10.1007/BF02692637.
[5] C.X. Zhu, C.L. Zhu, W.W. Zhao, et al., EXperimental study on the shear adhesion strength between the ice and substrate in icing wind tunnel, J. Mech. 34 (2) (2018) 209–216, https://doi.org/10.1017/jmech.2017.83.
[6] F. Caliskan, C. Hajiyev, A review of in-flight detection and identification of aircraft icing and reconfigurable control, Prog. Aeosp. Sci. 60 (2013) 12–34, https://doi.org/10.1016/j.paerosci.2012.11.001.
[7] J.Y. Lv, Y.L. Song, L. Jiang, et al., Bio-inspired strategies for anti-icing, Acs Nano. 8 (4) (2014) 3152–3169, https://doi.org/10.1021/nn406522n.
[8] M. Ruan, J.W. Wang, Q.L. Liu, et al., Superhydrophobic and anti-icing properties of sol-gel prepared alumina coatings, Russ. J. Non-Ferrous Metals. 57 (6) (2016)638–645, https://doi.org/10.3103/S1067821216060122.
[9] Y. Liu, L.Q. Ma, W. Wang, et al., An experimental study on soft pdms materials for aircraft icing mitigation, Appl. Surf. Sci. 447 (2018) 599–609, https://doi.org/10.1016/j.apsusc.2018.04.032.
[10] L.C. Shu, J. Liang, Q. Hu, et al., Study on small wind turbine icing and its performance, Cold Reg. Sci. Tech. 134 (2017) 11–19, https://doi.org/10.1016/j.coldregions.2016.11.004.
[11] E. Andenaes, B.P. Jelle, K. Ramlo, et al., The influence of snow and ice coverage on the energy generation from photovoltaic solar cells, Sol. Energy. 159 (2018) 318–328, https://doi.org/10.1016/j.solener.2017.10.078.
[12] B.P. Jelle, The challenge of removing snow downfall on photovoltaic solar cell roofs in order to maximize solar energy efficiency-Research opportunities for the future, Energy Build. 67 (2013) 334–351, https://doi.org/10.1016/j.enbuild.2013.08.010.
[13] T.K. Chen, J.F. Jin, Y.C. Qi, et al., Disturbing stability of interface by adopting phase-change temperature gradient to reduce ice adhesion strength, Cold Reg. Sci. Tech. 158 (2019) 69–75, https://doi.org/10.1016/j.coldregions.2018.11.010.
[14] T. Rashid, H.A. Khawaja, K. Edvardsen, Review of marine icing and anti-/de-icing system, J. Mar. Eng. Technol. 15 (2) (2016) 79–87, https://doi.org/10.1080/20464177.2016.1216734.
[15] S. Ronneberg, S. B. Xiao, J. Y. He, et al., Nanoscale correlations of ice adhesion strength and water contact angle, Coatings. 10 (4) (2020), ID 379. https://doi.org/10.3390/coatings10040379.
[16] P. Zhang, F.Y. Lv, A review of the recent advances in superhydrophobic surfaces and the emerging energy-related applications, Energy. 82 (2015) 1068–1087, https://doi.org/10.1016/j.energy.2015.01.061.
[17] P. O. A. Borrebaek, B. P. Jelle, Z. L. Zhang, Avoiding snow and ice accretion on building integrated photovoltaics–challenges, strategies, and opportunities, Sol. Energy Mater. Sol. Cells. 206 (2020), Article ID 110306. https://doi.org/10.1016/j.solmat.2019.110306.
[18] W. Tong, D. S. Xiong, N. Wang, et al., Mechanically robust superhydrophobic coating for aeronautical composite against ice accretion and ice adhesion, Compos. Pt. B-Eng. 176 (2019), Article ID 107267. https://doi.org/10.1016/j.compositesb.2019.107267.
[19] C. Antonini, M. Innocenti, T. Horn, et al., Understanding the effect of superhydrophobic coatings on energy reduction in anti-icing systems, Cold Reg. Sci. Tech. 67 (1–2) (2011) 58–67, https://doi.org/10.1016/j.coldregions.2011.02.006.
[20] M. Mohseni, A. Amirfazli, A novel electro-thermal anti-icing system for fiber-reinforced polymer composite airfoils, Cold Reg. Sci. Tech. 87 (2013) 47–58, https://doi.org/10.1016/j.coldregions.2012.12.003.
[21] A. Muthumani, L. Fay, M. Akin, et al., Correlating lab and field tests for evaluation of deicing and anti-icing chemicals: a review of potential approaches, Cold Reg. Sci. Tech. 97 (2014) 21–32, https://doi.org/10.1016/j.coldregions.2013.10.001.
[22] S. Ozbay, H.Y. Erbil, Ice accretion by spraying supercooled droplets is not dependent on wettability and surface free energy of substrates, Colloid Surf. A-Physicochem. Eng. Asp. 504 (2016) 210–218, https://doi.org/10.1016/j.colsurfa.2016.05.065.
[23] O. Parent, A. Llinca, Anti-icing and de-icing techniques for wind turbines: critical review, Cold Reg. Sci. Tech. 65 (1) (2011) 88–96, https://doi.org/10.1016/j.coldregions.2010.01.005.
[24] L. Oberli, D. Caruso, C. Hall, et al., Condensation and freezing of droplets on superhydrophobic surfaces, Adv. Colloid Interface Sci. 210 (2014) 47–57, https://doi.org/10.1016/j.cis.2013.10.018.
[25] H.K. Zheng, S.N. Chang, Y.N. Zhao, Anti-icing & icephobic mechanism and applications of superhydrophobic/ultra slippery surface, Prog. Chem. 29 (1) (2017) 102–118, https://doi.org/10.7536/PC161015.
[26] B. Bharathidasan, S.V. Kumar, M.S. Bobji, et al., Effect of wettability and surface roughness on ice-adhesion strength of hydrophilic, hydrophobic and superhydrophobic surfaces, Appl. Surf. Sci. 314 (2014) 241–250, https://doi.org/10.1016/j.apsusc.2014.06.101.
[27] J. Chen, J. Liu, M. He, et al., Superhydrophobic surfaces cannot reduce ice adhesion, Appl. Phys. Lett. 101 (2012), Article ID 111603. https://doi.org/10.1063/1.4752436.
[28] S. Farhadi, M. Farzaneh, S.A. Kulinich, Anti-icing performance of superhydrophobic surfaces, Appl. Surf. Sci. 257 (14) (2011) 6264–6269, https://doi.org/10.1016/j.apsusc.2011.02.057.
[29] S. Jung, M. Dorrestijn, D. Raps, et al., Are superhydrophobic surfaces best for icephobicity? Langmuir. 27 (6) (2011) 3059–3066, https://doi.org/10.1021/la104762g.
[30] S.A. Kulinich, S. Farhadi, K. Nose, et al., Superhydrophobic surfaces: are they really ice-repellent? Langmuir. 27 (1) (2011) 25–29, https://doi.org/10.1021/la104277q.
[31] M. Nosonovsky, V. Hejazi, Why superhydrophobic surfaces are not always icephobic, ACS Nano. 6 (2012) 8488–8491, https://doi.org/10.1021/nn302138r.
[32] T.M. Schutzius, S. Jung, T. Maitra, et al., Physics of icing and rational design of surfaces with extraordinary icephobicity, Langmuir. 31 (2015) 4807–4821, https://doi.org/10.1021/la502586a.
[33] K.K. Varanasi, T. Deng, J.D. Smith, et al., Frost formation and ice adhesion on superhydrophobic surfaces, Appl. Phys. Lett. 97 (2010), Article ID 234102. https://doi.org/10.1063/1.3524513.
[34] A. Lazauskas, A. Guobiene, I. Prosyevas, et al., Water droplet behavior on superhydrophobic SiO_2 nanocomposite films during icing/deicing cycles, Mater. Charact. 82 (2013) 9–16, https://doi.org/10.1016/j.matchar.2013.04.017.
[35] R. Jain, R. Pitchumani, Facile fabrication of durable copper-based superhydrophobic surfaces via electrodeposition, Langmuir. 34 (2018) 3159–3169, https://doi.org/10.1021/acs.langmuir.7b02227.
[36] M. Villegas, Y.X. Zhang, N. Abu Jarad, et al., Liquid-infused surfaces: a review of theory, design, and applications, ACS Nano. 13 (2019) 8517–8536, https://doi.org/10.1021/acsnano.9b04129.
[37] S.L. Zheng, C. Li, Q.T. Fu, et al., Development of stable superhydrophobic coatings on aluminum surface for corrosion-resistant, self-cleaning, and anti-icing

applications, Mater. Des. 93 (2016) 261–270, https://doi.org/10.1016/j.matdes.2015.12.155.
[38] A.R. Parker, R.C. Lawrence, Water capture by a desert beetle, Nature. 414 (6859) (2001) 33–34, https://doi.org/10.1038/35102108.
[39] L.Q. Ren, Progress in the bionic study on anti-adhesion and resistance reduction of terrain machines, Sci. China Ser. E-Technol. Sci. 52 (2) (2009) 273–284, https://doi.org/10.1007/s11431-009-0042-3.
[40] L.Q. Ren, Y.H. Liang, Biological couplings: classification and characteristic rules, Sci. China Ser. E-Technol. Sci. 52 (2009) 2791–2800, https://doi.org/10.1007/s11431-009-0325-8.
[41] L.Q. Ren, Y.H. Liang, Biological couplings: function, characteristics and implementation mode, Sci. China-Technol. Sci. 53 (2010) 379–387, https://doi.org/10.1007/s11431-010-0043-2.
[42] L.Q. Ren, Y.H. Liang, Preliminary studies on the basic factors of bionics, Sci. China-Technol. Sci. 57 (2014) 520–530, https://doi.org/10.1007/s11431-013-5449-1.
[43] L.Q. Ren, Y.H. Liang, The Introduction of Bionics, 1st ed., China Science Publishing & Media. Ltd, China, Beijing, 2016.
[44] R.M. Fillion, A.R. Riahi, A. Edrisy, Design factors for reducing ice adhesion, J. Adhes. Sci. Technol. 31 (2) (2017) 2271–2284, https://doi.org/10.1080/01694243.2017.1297588.
[45] H. Memon, J. P. Liu, D. S. A. De Focatiis, et al., Intrinsic dependence of ice adhesion strength on surface roughness, Surf. Coat. Technol. 385 (2020), Article ID 125382. https://doi.org/10.1016/j.surfcoat.2020.125382.
[46] J. F. Jin, Y. Y. Chen, Y. C. Qi, et al., Changes in the interfacial stress of water on aluminum alloy surface during the freezing and thawing process, Cold Reg. Sci. Tech. 194 (2022), Article ID 103460. https://doi.org/10.1016/j.coldregions.2021.103460.
[47] G.Q. Lai, Organic Silicon Chemistry and Technology, 1st ed., Chemical Industry Press Co., Ltd, China, Beijing, 2011.
[48] S.S. Xie, J.A. Liu, J. Xu, et al., Concise Aluminum Alloy Processing Manual, 1st ed., Metallurgical Industry Press Co., Ltd, China, Beijing, 2016.
[49] ASTM D3359, 2017. Standard test methods for rating adhesion by tape test [S].
[50] G. Chaudhary, R. Li, Freezing of water droplets on solid surfaces: an experimental and numerical study, Exp. Therm. Fluid Sci. 57 (2014) 86–93, https://doi.org/10.1016/j.expthermflusci.2014.04.007.
[51] Q. Cong, J. Xu, L.Q. Ren, et al., Changes of water/ice morphological, thermodynamic, and mechanical parameters during the freezing process, Arab. J. Sci. Eng. 46 (2021) 10631–10639, https://doi.org/10.1007/s13369-021-05502-0.
[52] S. Tabakova, F. Feuillebois, On the solidification of a supercooled liquid droplet lying on a surface, J. Colloid Interface Sci. 272 (2004) 225–234, https://doi.org/10.1016/j.jcis.2003.10.029.
[53] Q. Xu, Z.Y. Li, J. Wang, Characteristics of single droplet impact on cold plate surfaces, Dry. Technol. 30 (2012) 1756–1762, https://doi.org/10.1080/07373937.2012.708001.
[54] H. Hui, Z.Y. Jin, An icing physics study by using lifetime-based molecular tagging thermometry technique, Int. J. Multiph. Flow. 36 (2010) 672–681, https://doi.org/10.1016/j.ijmultiphaseflow.2010.04.001.